Autonomous Recovery of a Fixed-Wing UAV Using a Net Suspended by Two Multirotor UAVs

Kristian Klausen, Thor I. Fossen, Tor Arne Johansen
Department of Engineering Cybernetics
NTNU Centre for Autonomous Marine Operations and Systems
Norwegian University of Science and Technology, NTNU
Trondheim, Norway
kristian.klausen@ntnu.no

Abstract

This article presents a novel recovery method for fixed-wing Unmanned Aerial Vehicles (UAVs), aimed at enabling operations from marine vessels. Instead of using the conventional method of using a fixed net on the ship deck, we propose to suspend a net under two cooperative multirotor UAVs. While keeping their relative formation, the multirotor UAVs are able to intercept the incoming fixed-wing UAV along a virtual runway over the sea, and transport it back to the ship. In addition to discussing the concept and design a control system, this paper also presents experimental validation of the proposed concept for a small-scale UAV platform.

1 Introduction

Fixed-Wing Unmanned Aerial Vehicles have a vast range of use-cases. Mostly, these encompass surveillance or other form of remote sensing. The fixed-wing UAV is the natural choice for a UAV in many of these cases, due to their long range, high endurance and flexible payload capacity.

The maritime sector has a need to operate these types of UAVs. They would like to use UAVs for ice surveying and monitoring, scan for unidentified vessels, search and rescue, and to provide extended range for survey-missions normally conducted from shore. Key challenges that needs to be addressed for autonomous operations are takeoff and landing (recovery) of the UAV. For takeoff, the use of catapults, powered by pneumatics, springs or rubber bands, has proven to be a useful tool that is applicable to many types of airframes and operation-types. Autonomous recovery is, however, an active area of research.

Several aspects of autonomous landing of fixed-wing UAVs are discussed in the literature. In (Rife et al., 2008), a navigation system with emphasis on robustness and accuracy is presented by utilizing dual-frequency, carrier phase differential GNSS. The authors also proposes solutions to some of the challenges associated with local antenna arrays for jamming prevention and fault monitoring strategies. Autonomous landing in a fixed-net is demonstrated in (Skulstad et al., 2015), using lower cost single frequency carrier-phase RTK GPS with successful experimental validation. (Muskardin et al., 2017) uses a combination of GNSS and vision systems to reliably land a fixed-wing UAV on a moving car, intended to be used as a recovery platform for larger high altitude, long endurance UAVs without heavy landing gear. Pure vision-based navigation systems for autonomous fixed-wing UAV landing is tried in (Thurrowgood et al., 2014), (Laiacker et al., 2013) and (Kim et al., 2013).

Recovery of Fixed-Wing UAVs from ships require different methodologies from those performed on shore. There are several challenges associated with such operations, including heave-induced motion from waves, turbulence near the ship, and the safety of the crew operating on deck. In addition, there is no room for a runway unless it is a ship dedicated to such operations. Instead, most operations rely on the dissipative effects of a fixed net or wires and hooks to stop the incoming UAV. Vertical Take-Off and Landing (VTOL) UAVs does not require such infrastructure, but still requires accurate positioning and tracking to be able to reliably land on moving targets such as ships. Such operations are addressed in (Richardson et al., 2013), (Venugopalan et al., 2012) and (Serra et al., 2016), using vision system for navigational aid during the final descent.

Figure 1: Image from the experimental validation. The fixed-wing UAV is approaching the net, which is being carried by two multirotor UAVs. On the right, the fixed-wing UAV is arrested by the net, and stays attached due to hooks on the nose of the UAV.

In this paper, we present a novel approach for landing a small fixed-wing UAV for maritime missions. By suspending a net below two multirotor UAVs, the entire recovery operation can be moved off deck. The fixed-wing UAV is equipped with hooks so that after impact with the net, it will be arrested by the net to be transported back to the ship. Figure 1 shows the recovery system in action, and Figure 2 illustrates the sequence of events when recovering a fixed-wing UAV from a ship.

Recovery of UAVs with nets suspended by multirotors have been attempted in various settings. Due to the popularity of consumer-type multirotor UAVs, there is an increased interest in the ability to safely remove such vehicles from restricted airspaces. In (Delftdynamics.nl, 2015), a multirotor is equipped with a net gun, capable of incapacitating smaller multirotors by shooting a net at them to disable the rotors on the target. A similar experiment was conducted in (Mtu.edu, 2016), where the target multirotor stays attached to the larger multirotor after the net is fired, see also (Theverge.com, 2015), (Nextgenerationvision.fr, 2014). To the best of the authors knowledge, no attempts at cooperative recovery of fixed-wing UAVs in a net suspended between multirotor UAVs have yet been published.

The contributions of this paper is the experimental validation and functional description of the system first reported in (Klausen et al., 2016). In addition to some changes in the controllers, we outline the implementation steps. The experiments were conducted in december 2016, using a small fixed-wing UAV (1.5 kg). An image of the experiment under-way can be seen in Figure 1.

1.1 Organization

The article is organized as follows. In Section 2, the autonomous net recovery is introduced, and key aspects and advantages are discussed. Further, the definition of the *virtual runway* is given in Section 2.4. Section 3 presents the proposed control design, which includes coordination controllers between the multirotor UAVs and the incoming fixed-wing UAV. The experimental platform is given in Section 4, which in addition to introducing the hardware and software, also details the operational procedure and safety considerations considered when performing the experiments. The results of the trials are presented in Section 5, followed by concluding remarks in Section 6.

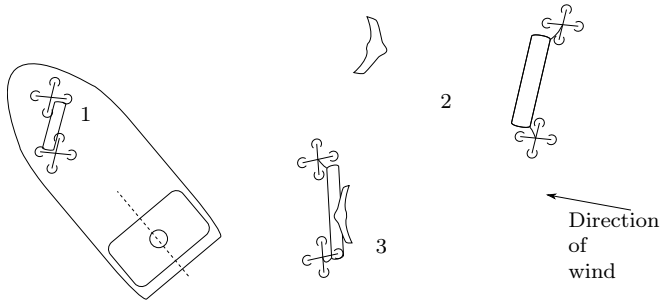

Figure 2: The figure illustrates the recovery of a fixed-wing UAV. (1), the multirotors take off from the ship. (2), the fixed-wing UAV moves against the wind direction, while the multirotors position the net along a virtual runway (coinciding with the fixed-wing UAV trajectory) and accelerate to a prescribed velocity in order to catch the incoming fixed-wing UAV. (3), the multirotors are transporting the fixed-wing UAV back to the ship.

2 Autonomous Net Recovery

In this section, the concept of UAV recovery using a net suspended below multirotors is discussed in further details. As described in (Klausen et al., 2016) in the context of ship-based UAV operations, key benefits of the proposed approach are

- *Operational flexibility:* When recovering a fixed-wing UAV, it is usually beneficial to travel against the wind to minimize the ground speed, and thus a fixed net should be aligned with this path. Even in vessels equipped with Dynamic Positioning (DP) systems, turning the ship can be undesirable as it may interfere with operations. The multirotors can however quickly react to changing wind conditions, and align the net against the wind without the need to coordinate with other ship operations.
- *Not affected by waves and turbulence:* Since the net is suspended away from the ship, heave motion induced by waves on the ship will not affect the landing. Also, there is no impact from turbulence caused by the ship super-structure.
- *Safety:* By having the net suspended by two multirotor UAVs, the recovery operation can be moved off ship. Thus, no operators or staff risk coming in contact with the incoming UAV.
- *Smaller impact force:* By having the two multirotors move away from the fixed-wing UAV, the relative speed difference between it and the net can be made smaller, thus decreasing the structural load on the fixed-wing body during impact.
- *Smaller footprint:* By moving the landing operation off ship, operations with UAVs can be conducted from smaller ships, not needing a large open deck with a net to support the mission. Launch and recovery of the multirotors are still required.

These benefits are useful also in other recovery scenarios where there is limited space available.

Autonomous recovery of a fixed-wing UAV in a suspended net is a complex task, so the functionality is split into several components. The fixed-wing UAV is commanded to follow a path against the wind, with the minimal airspeed required for safe flying. This path is called the *virtual runway*, and the path is transmitted to the multirotor UAVs. Both multirotors are equipped with coordinated controllers that keep the inter-formation of the two intact, while lifting the suspended net. The current position and the velocity of the fixed-wing UAV is transmitted in real-time at regular intervals to a coordination controller in one of the multirotors, which sends desired setpoints to the formation controllers according to the phases of the mission, as to catch the fixed-wing UAV. An overview of the components and their communication can be seen in Figure 3.

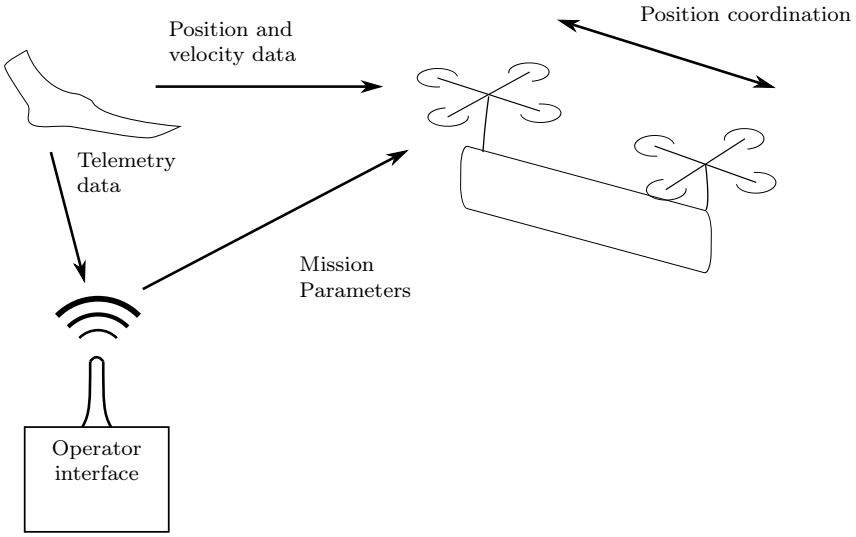

Figure 3: Simplified overall overview of the system. The operator specifies the location of the *Virtual Runway*, based on weather conditions, air space regulations and the surroundings. This instructs the multirotors to wait at the start of the virtual runway, while monitoring the position of the incoming fixed-wing UAV to initiate the recovery maneuver. Low-level controllers synchronize the relative formation of the multirotors, to position the net at the correct position and orientation.

Although using two multirotor UAVs instead of one increases the complexity of the system, it has several practical advantages. First, by distributing the load, each multirotor can be physically smaller than a single multirotor with the combined lift capacity. This can lead to simplified operations, and makes it easier to have redundancy in the equipment. Further, although not utilized in this research, the two multirotors can spread the net without a support structure (top beam), giving reduced weight and high stability of the net.

2.1 The Recovery Maneuver

The maneuver is composed by the following key steps:

1. **Initialization:** The operator specifies the location and direction of the desired recovery point by defining the *Virtual Runway* (VR). This runway defines the desired path of the incoming fixed-wing UAV. The operator defines the safety area around the runway (that is, how far away from the center line can the multirotors go while tracking the fixed-wing UAV), and other parameters such as desired relative recovery velocity.
2. **Standby:** The multirotors take off, and lift the net toward the start of the virtual runway. They

are now waiting for the incoming fixed-wing UAV to approach.

3. **Approach:** When the fixed-wing UAV is approaching, the multirotors starts to align themselves with the location of the fixed-wing UAV in the cross-track plane of the virtual runway. This is typically 10 s prior to impact, and the tracking is in a *low-gain mode* to not over-react unnecessarily to the movements of the fixed-wing UAV as it is approaching.

4. **Start:** Based on the speed on the incoming fixed-wing UAV and desired relative speed, the multirotors starts to move along the virtual runway with a prescribed velocity and acceleration profile as to intercept the fixed-wing UAV at the desired recovery point. The multirotors are able to accelerate quite fast, so the desired speed is achieved quickly. At this point, the multirotors track the location of the fixed-wing UAV with a *higher gain* and agility, typically 3-5 s before the recovery time.

5. **Catch:** The multirotors are continuously monitoring the state of the incoming fixed-wing UAV, and tracks it's location until a successful catch is detected. If at any point the tracking is off or communication is lost, the multirotors can initiate a evasive maneuver and restart the recovery phase by instructing the fixed-wing to loop back and do another attempt.

6. **Return:** After the catch, the fixed-wing UAV stays attached to the net due to hooks and other edged structures, and is safely transported back by the multirotors which land individually after releasing the net.

After a successful recovery, the multirotor UAVs will need to land on a (possibly moving) vessel with the suspended fixed-wing UAV attached in the net. Although this is a non-trivial operation, the nature of the multirotor dynamics allow for hover and fast responses to synchronize with the dynamics of the heaving vessel. Such approaches has previously been studied in e.g. (Venugopalan et al., 2012; Serra et al., 2016).

2.2 Navigation

Precise navigation is crucial for precision landing of UAVs. In this work, we utilize *Real-Time Kinematic* (RTK) *Global Navigation Satellite System* (GNSS). This is a navigation technique using the carrier wave of the incoming signals from the satellites, and comparing the signals to that received by a base station. By computing the phase shift between the signals at the UAV (rover) and the base, the location can be locked in at centimeter-level accuracy. Such a system was used in (Skulstad et al., 2015) for landing a fixed-wing UAV in a stationary net, which also contains more detailed information about RTK GNSS systems. When locating the RTK GNSS base on the moving ship, care must be taken if the ship is moving. However, by operating the system in a *moving baseline* configuration, the *relative* accuracy between the Fixed-wing UAV and Multirotor UAVs will be unchanged, and the moving base position can be corrected for by either traditional GNSS localization or by a land-based GNSS base station.

2.3 Emergency Plans

The design of the recovery maneuver readily makes it possible to design various emergency plans to be executed at different phases of the maneuver, as discussed in Section 2.1. The maneuver can be halted at any point without risk of damage, even near the point of recovery. By continuously monitor the available data, emergency plans can be executed in the case of communication errors or loss of navigation solutions. Such plans can include repositions of the multirotors and waiting-patterns for the fixed-wing. In severe error cases, for instance if the multirotor UAVs are unable to maintain their desired formation positions due to mechanical faults or complete loss of satellite reception coverage, the suspended net can be released from the suspension points.

2.4 Virtual runway

Figure 4 illustrates the *virtual runway* (VR). The virtual runway is used by the operator to set a designated area for the recovery maneuver. In addition, the operator an specify boundaries in the vertical and lateral direction of the runway, working as a virtual fence for the location of the multirotor UAVs. The virtual runway defines a path-frame, which is again divided into a *cross-track* plane and an *along-track* distance, so we can design controllers for each part separately.

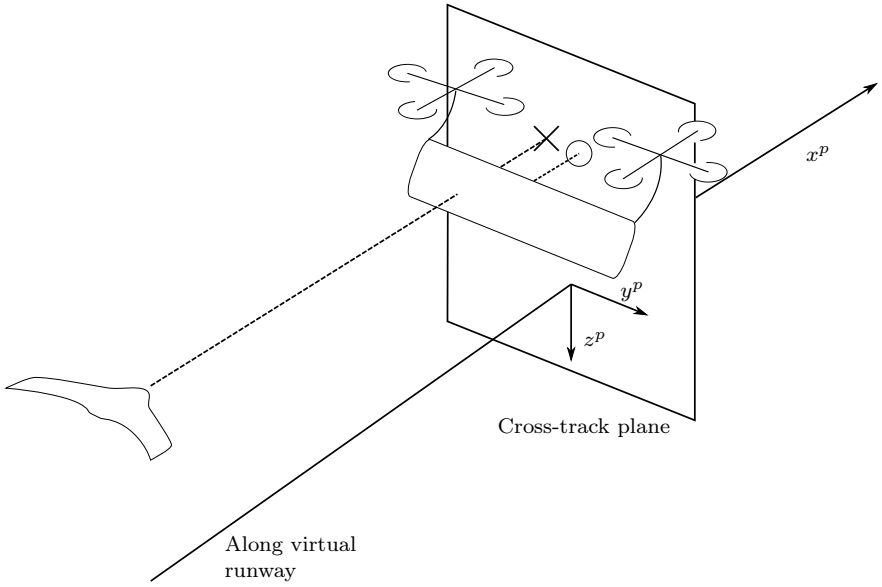

Figure 4: Illustration of the *virtual runway*. The runway defines a *path coordinate frame* $\{p\}$, and can be divided into a cross-track plane ($y^p z^p$) and an along-track distance x^p. The center position of the net on the cross-track plane is marked with a circle, while the intersection of the cross-track plane and the path of the fixed-wing UAV is marked with a cross.

3 Control design

This section introduces the control design, and gives details about each of the different parts. The overall structure can be seen in Figure 5. There are three distinct control modules, namely a *Coordination controller*, which uses information from the incoming fixed-wing UAV to intercept and recovery it, by sending setpoints to the underlying *multirotor formation controller*. A *supervisory controller* tracks the current overall state of the maneuver. All three are further discussed in the next sections. The *Virtual Runway* formally defines a path coordinate frame $\{p\}$ at constant altitude, which is defined by an origin $\mathbf{p}^n_{p/n}$ and a rotation ψ around the $\{n\}$ z-axis such that $\mathbf{R}^n_p = \mathbf{R}_z(\psi)$. Then a position $\mathbf{p}^n$ can be decomposed in $\{p\}$ by the transformation $\mathbf{p}^p = (\mathbf{R}^n_p)^{\mathrm{T}}(\mathbf{p}^n - \mathbf{p}^n_{p/n})$. Further, the frame is divided into a *cross-track* plane and an *along-track* distance, for which coordination controllers are developed individually.

3.1 The Fixed-Wing UAV Autopilot

The fixed-wing is equipped with an autopilot, taking care of all local navigation and control tasks with the accuracy of a standard code-based GNSS solution. For the recovery maneuver, the fixed-wing UAV receives information about the virtual runway from the operator, specifying altitude and reference air speed. Information about position and velocity is continuously transmitted to both the operator as telemetry data and to the multirotor autopilots. The detailed aspects of guidance and control of a fixed-wing UAV is

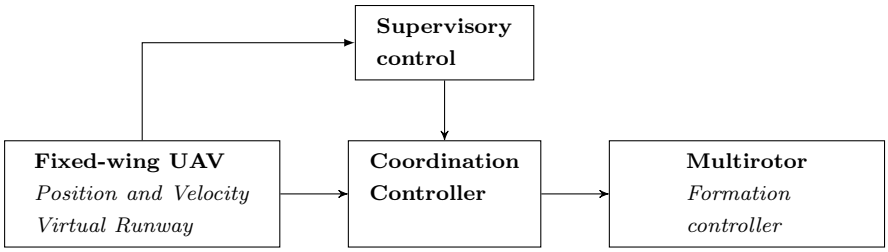

Figure 5: Information flow in the controller structure. Based on the current position of the fixed-wing UAV, the supervisor starts the net-recovery maneuver. The coordination controller guides the two multirotors along a virtual runway to intercept the fixed-wing UAV.

thoroughly addressed in the literature (for instance (Beard and McLain, 2012)) and is not within the scope of this paper.

3.2 Multirotor Control

Modeling and control of a multirotor UAV has been thoroughly studied in the literature. For a detailed survey, refer to (Mahony et al., 2012) and references therein. In this context, we are interested in the translational dynamics, and assume that an autopilot with a low-level controller is present on the UAV.

In the following, let the subscript $(\cdot)_i$ denote the i'th multirotor. It's dynamics is governed by

$$m_i \dot{\mathbf{v}}_i = m_i \mathbf{g} + \mathbf{R}_i \vec{e}_3 f_i + \boldsymbol{\tau}_{L,i} \tag{1}$$

where m_i is the vehicle mass, $\mathbf{v}_i \in \mathbb{R}^3$ the velocity in a local North-East-Down (NED) frame $\{n\}$, assumed inertial, $\mathbf{g}$ is the gravitation acceleration vector $[0,\, 0,\, g]^{\mathrm{T}}$, where g is the gravitational constant. The orientation or the multirotor, specified by the body-aligned reference frame $\{b\}$, is represented with $\mathbf{R}_i \in \mathcal{SO}^3$. This orientation is crucial to the behavior of the multirotor, as it is can only apply thrust, $f_i \in \mathbb{R}$, along the z-axis ($\vec{e}_3$). External forces, such as the load from the suspended net and environmental effects, is given in $\boldsymbol{\tau}_{L,i} \in \mathbb{R}^3$.

The direction of applied force is given by $\mathbf{R}_i$, which corresponds to specifying the roll- and pitch-angle of the vehicle. Since we assume a sufficiently fast low-level attitude controller is present on the multirotor UAV is present (examples of such is given in (Mahony et al., 2012) and (Klausen et al., 2014)), the term $\mathbf{R}_i \vec{e}_3 f_i$ can be replaced by an inertial control force $\mathbf{F}_i \in \mathbb{R}^3$, resulting in the dynamics

$$m_i \dot{\mathbf{v}} = m_i \mathbf{g} + \mathbf{F}_i + \boldsymbol{\tau}_{L,i} \tag{2}$$

3.2.1 Formation control

The design of the formation controller between the multirotor UAVs is based on a passivity design as presented in (Arcak, 2007) and (Bai et al., 2011). Each of the copters are *synchronizing* their relative position, meaning that both multirotors actively maintain their desired configuration by using position and velocity measurement from themselves and the other vehicle. Both vehicles receive a common *mission velocity*, which drives the position of the multirotors in the inertial coordinate frame. In addition, each multirotor has an internal adaptive scheme to compensate for the unknown disturbance $\boldsymbol{\tau}_{L,i}$ from the suspended net. The

structure of the formation controller can be seen in Figure 6. More details about the controller, including Lyapunov-based stability proofs, can be found in (Meissen et al., 2017) and (Klausen et al., 2016).

The mission velocity $\mathbf{v}^d$ provided to the formation controller must be a smooth, differentiable signal. Formally, let a signal have $\mathcal{C}^n$ continuity if the nth derivative are continuous. To account for the time it takes for the multirotor to realize a desired force output by adjusting its roll- and pitch angle, a $\mathcal{C}^2$ signal is desirable.

Next, the coordination controller, which supplies the mission velocity to the multirotors, is discussed.

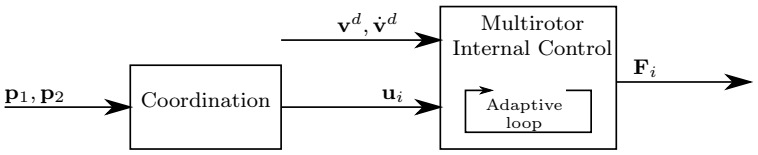

Figure 6: The overall structure of the relative *synchronization* between the multirotors. By using available positions from each other $\mathbf{p}_1, \mathbf{p}_2$, the multirotors cooperatively reach their desired relative position. Internally, each multirotor is applying an *adaptive control* scheme to counter-act the unknown disturbances from the suspended net. An external controller supply the common *mission velocity* signal $\mathbf{v}^d$.

3.3 Fixed-Wing and Multirotor Coordination

To be able to recover the fixed-wing UAV with the net suspended below the multirotors, some level of coordination is needed between the vehicles. Various control strategies were considered, where on one end the fixed-wing UAV should control itself as to hit the net, and on the other the fixed-wing UAV simply followed its nominal flight path and the multirotors did all the tracking. These two strategies could also be combined to a synchronized maneuver.

In the end, we settled on letting the agile multirotors do most of the coordination. This has the advantage of letting the fixed-wing UAV keep a stable, clean flight path rather than correcting minor deviations from the net position. It simplified the control and hardware design, and issues such as time delays in the communication are less pronounced. Thus, from a control-design point of view, the fixed-wing UAV acts as a reference generator, or master, to the coordination controllers on the multirotor UAVs.

In the next sections, let $\mathbf{p}_i^n \in \mathbb{R}^3, i \in \{1, 2\}$ be the position of multirotor i in the inertial coordinate frame $\{n\}$. Further, we define the position $\bar{\mathbf{p}}^n := (\mathbf{p}_1^n + \mathbf{p}_2^n)/2 + \mathbf{p}_{offset}^n$ as the centroid of the two multirotors plus an height offset to compensate for the position of the net. Further, the states of the fixed-wing UAV is denoted with subscript $\cdot_f$.

3.3.1 Coordination - Cross-track

The position of the net is controlled according to the fixed-wing UAV position in the cross-track plane along the virtual runway. A cross-track frame $\{p_*\}$ is defined as the yz-plane in the path frame $\{p\}$, such that there exist a mapping from a position $\mathbf{p}^p = \begin{bmatrix} p_x & p_y & p_z \end{bmatrix}^\mathrm{T}$ to $\mathbf{p}^{p_*} = \mathbf{p}_{2:3}^p = \begin{bmatrix} p_y & p_z \end{bmatrix}^\mathrm{T} \in \mathbb{R}^2$.

To generate smooth $\mathcal{C}^2$ signals to the low-level multirotor controllers, where a signal has $\mathcal{C}^n$ continuity if the nth derivative are continuous, the navigation data from the fixed-wing is fed through a tracking generator. This ensures continuity and smoothness of the reference signals. Let the generator be governed by the dynamics of a third-order filter:

$$\mathbf{x}^{(3)} + (2\zeta + 1)\omega_0 \ddot{\mathbf{x}} + (2\zeta + 1)\omega_0^2 \dot{\mathbf{x}} + \omega_0^3 \mathbf{x} = \omega_0^3 \mathbf{p}_f^{p_*} \tag{3}$$

where $\omega_0, \zeta \in \mathbb{R}$ are tuning parameters. To further enhance the tracking results, the measured velocity from the fixed-wing UAV $\mathbf{v}_f^p$ is used as a feed forward in the trajectory generation. In addition, to be able to prescribe maximum setpoint velocities and accelerations, (3) is re-written as a third-order integrator with saturating elements as illustrated in (Klausen et al., 2017):

$$\mathbf{x}^{(3)} = \mathbf{u} \tag{4}$$

$$\tau_1 = \mathrm{sat}(\mathrm{k}_1(\mathbf{p}_\mathrm{f}^{\mathrm{p}*} - \mathbf{x}), \mathrm{v}_{\max}) \tag{5}$$
$$\tau_2 = \mathrm{sat}(\mathrm{k}_2(\tau_1 + \mathbf{v}_\mathrm{f}^{\mathrm{p}*} - \mathbf{x}^{(1)}), \mathrm{a}_{\max}) \tag{6}$$
$$\mathbf{u} = k_3(\tau_2 - \mathbf{x}^{(2)}) \tag{7}$$

The parameters $k_i, i \in \{1, \ldots, 3\}$ are found by inspection of (3) as

$$k_3 = (2\zeta + 1)\omega_0 \qquad k_2 = \frac{(2\zeta + 1)\omega_0^2}{k_3} \qquad k_1 = \frac{\omega_0^3}{k_3 k_2}$$

Similar techniques are described in (Teel, 1992; Arcak et al., 2001) Additionally, the virtual runway defines a boundary that the net should be within. The boundary fulfills a safety requirement in terms of defining the area where the landing will take place, and also gives the operator greater control. For the tracking, when the fixed-wing is outside of the boundary, the tracking generator uses the closest boundary to the virtual runway as the target position. In this case, the feed-forward from the measured fixed-wing velocity $\mathbf{v}_f$ is disabled. Figure 7 sums up the tracking generator.

Smooth $\mathcal{C}^3$ signals are preferable to the low-level formation controller, but to get adequate performance at the final parts of the recovery maneuver it is possible to reduce the model above to a second order one, leading to faster tracking performance. This is achieved by setting $k_3 = 0$ above and replacing (4) with $\ddot{\mathbf{x}} = \tau_2$, as illustrated by the dashed box in Figure 7.

The desired velocity $\mathbf{v}_d^{p_*}$ for the multirotors are now calculated by

$$\mathbf{v}_d^{p_*} = \dot{\mathbf{x}} + \mathbf{K}_p(\mathbf{p}^{p_*} - \mathbf{x}) \tag{8}$$

where also $\ddot{\mathbf{x}}$ is used directly as a feed-forward in the underlying controller.

It should be noted that the net position is not measured explicitly, and furthermore it is not a desirable control target as the net will swing during the transit. Therefore we seek to control the position $\bar{\mathbf{p}}$ as illustrated in Figure 4 as the circle in the cross-track plane. Hence, $\mathbf{p}^{p_*} = \bar{\mathbf{p}}_{2:3}$.

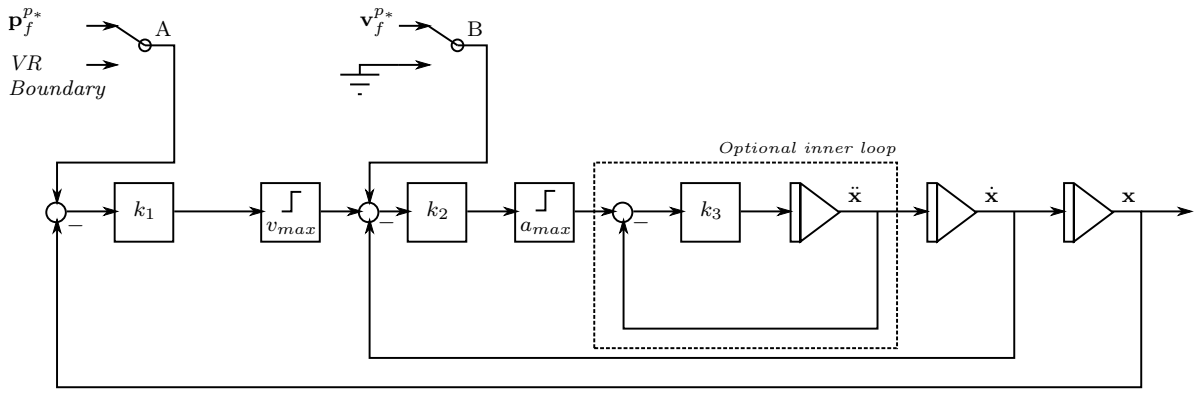

Figure 7: Block-diagram of the trajectory generator. The measured signals from the incoming fixed-wing UAV is filtered through the tracking algorithm to generate smooth reference signals to the controller. Based on the location of the fixed-wing UAV, the switches A and B can be set to adjust for the situation when the fixed-wing UAV is outside of the virtual runway. Note that the saturation blocks are not in between the integrators, ensuring consistent $\mathcal{C}^3$ signals. However, if faster performance is needed and $\mathcal{C}^2$ is sufficient at certain stages of the maneuver, the inner loop can be removed.

3.3.2 Coordination - Along-track

The relative velocity between the net and the fixed-wing UAV is reduced by accelerating the net to a desired velocity. In order to control the point of impact an, open loop scheme is proposed.

For the final recovery phase, the along-track velocity of the fixed-wing UAV is assumed constant. The virtual runway defines a point r_c along the runway as the designated recovery point. While waiting at the start of the virtual runway, the multirotor UAVs should monitor the location of the fixed-wing UAV. Based on a operator-defined relative speed to be achieved by the multirotors at the point of recovery r_c, the multirotor UAVs will start a pre-defined velocity profile along the virtual runway, to intercept the incoming fixed-wing UAV at r_c. By knowing the type of velocity profile used, the distance to the fixed-wing UAV, r_0, can be calculated based on the desired relative speed and along-track velocity of the fixed-wing UAV. This is summarized in Figure 8.

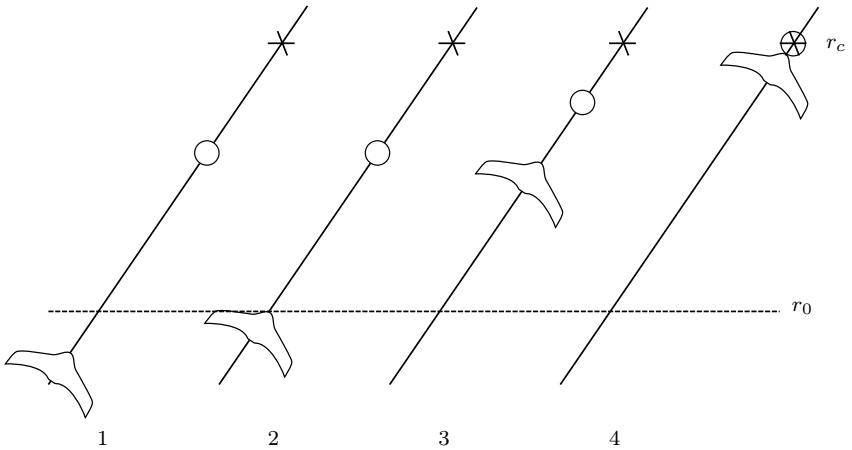

Figure 8: The figure shows the timing of the along-track velocity, where the current position of the net is marked with a circle at different instances of time (1)-(4). When the fixed-wing UAV reaches r_0, the multirotors starts the velocity profile for forward flight as to recover the fixed-wing UAV at r_c.

Different methods can be used to create a feasible velocity profile as the ultimate goal is to be able to calculate r_0. For the experimental setup conducted in this paper, a linear velocity profile with constant acceleration is utilized. As the acceleration phase of the along-track profile is rather quick for the agile multirotors, this proved more than sufficient. More elaborate profile could obviously be used, for instance the $\mathcal{C}^4$ polynomial profile proposed in (Klausen et al., 2016).

3.4 Supervisor

The supervisor monitors the position and velocity of the fixed-wing UAV relative to the virtual runway in order to switch between the different modes in the maneuver, as described in Section 2.1. Each mode enables a certain controller and reference which gives a desired velocity setpoint. The overall controller structure is thus summarized in Figure 9, where we see how the supervisor controls when to activate the various parts of the coordination controllers.

In addition, the supervisor monitors the maneuver as it is progressing. If, because of wind or other factors, the fixed-wing UAV misses the net, it instructs the vehicles to try the maneuver again. Furthermore, if the projected proximity of the fixed-wing UAV and multirotors are to small, the supervisor can abort the operation. Depending on the situation, an abort can involve the multirotors to climb and reposition for a retry, or releasing the net and abort the mission entirely.

Let $v^p_{d,x}(t)$ be the along-track velocity profile, designed as discussed in Section 3.3.2. By combining this with the desired velocity from the cross-track control, we get $\mathbf{v}^p_d = [v^p_{d,x}(t),\, (\mathbf{v}^{p_*}_d)^{\mathrm{T}}]^{\mathrm{T}}$, and the resulting desired velocity in $\{n\}$ can be found by the following transformation

$$\mathbf{v}^n_d = (\mathbf{R}^p_n)^{\mathrm{T}} \mathbf{v}^p_d \tag{9}$$

which gives the desired mission velocity for the two multirotors as discussed in Section 3.2.1. The complete controller structure is illustrated in Figure 9.

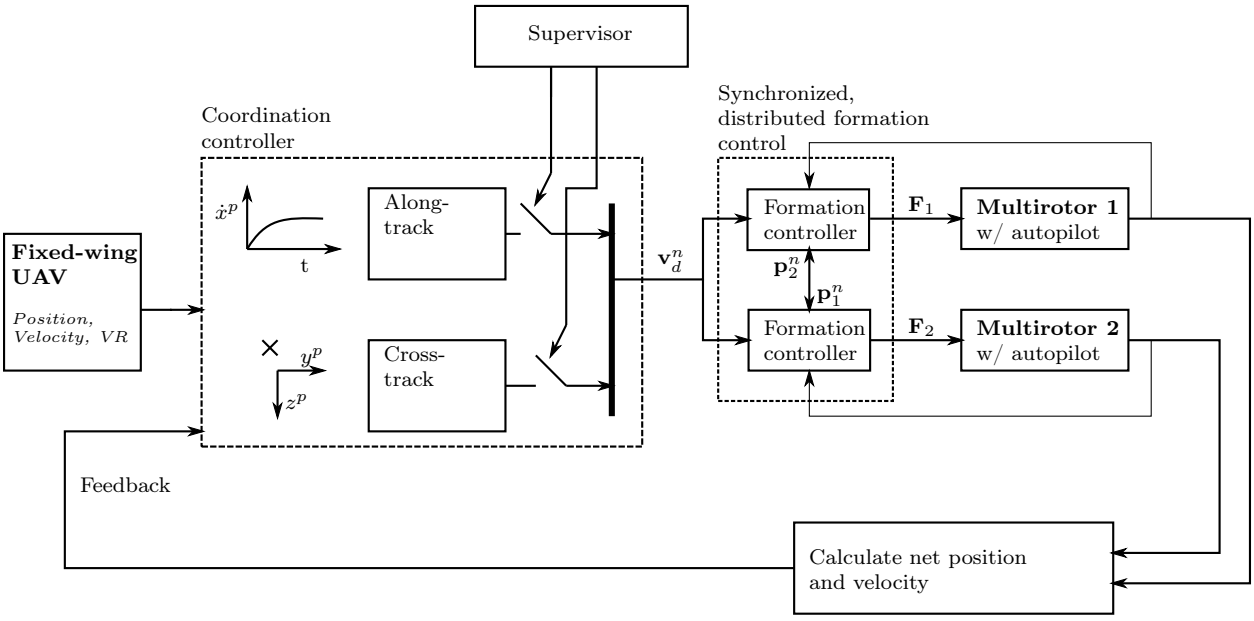

Figure 9: Illustration of the control-structure. The cross-track controller gets feedback from the position of the fixed-wing UAV in a plane orthogonal to the virtual runway. The along-track controller is an open-loop controller, initiated by the supervisor when the fixed-wing UAV reaches the virtual runway.

Table 1: Experimental platform

Multirotor UAV weight	2.2 kg
Fixed-wing UAV weight	1.2 kg
Fixed-wing UAV cruise speed	15 m/s
Fixed-wing UAV approach speed	12 m/s

4 Experimental Validation

To validate the concept illustrated above, a series of experiments were conducted with a platform of relatively small size vehicles. The fixed-wing UAV used for experiments are a modified hobby-grade RC plane, with a takeoff-weight of approx. 1.2 kg, and a cruise-speed of around 15 m/s. The multirotors weigh approx. 2.2 kg, and have enough lift capacity to lift the fixed-wing UAV, the net and necessary payloads. The following sections will discuss the various practical aspects with the implementation, such as the overall system architecture, choice of net and structural support systems, and the sensors needed. Finally, we will go over the operational aspect and the safety mechanisms built into the system. These parameters are summarized in Table 1.

Note that even though the UAVs in question can be considered relatively small, it is important to realize that all the functionality and solutions discussed in this section can be transferred to larger vehicles. The simulation study conducted in (Klausen et al., 2016) used a fixed-wing UAV with a maximum take-off weight of 4.2 kg, and multirotors with a total of 11 kg lifting capacity.

4.1 Overall System Architecture

The system consist of three main components; the fixed-wing UAV, the multirotors carrying the net, and a ground control segment. The ground control segment is used by the operators to configure the mission, and for monitoring and control during execution as discussed in Section 4.4. The fixed-wing UAV continuously sends position and velocity data to the multirotors, which calculates the path for interception when initiated by the operator. Even though the multirotors synchronize their position to achieve relative formation between themselves, the tracking- and coordination controllers described above runs on one of the multirotors, acting as a master.

Further, the system is designed to have a minimal impact on the normal operation of the fixed-wing UAV. Only a small module, consisting of an RTK GPS antenna, RTK GPS receiver and a wireless transmitter is required to be placed in the UAV. These components enable the accurate position and velocity of the fixed-wing UAV to be available on the controllers running on the multirotors.

4.2 Software and Hardware Platform

Each of the UAVs (both the fixed-wing and multirotors) are equipped with a Pixhawk (Pixhawk.ethz.ch, 2016) autopilot running the Ardupilot (Ardupilot.com, 2016) software stack. The autopilot handles navigation and low-level control of the vehicles, and for the fixed-wing UAV it also handles the guidance tasks. These autopilot's are based on highly flexible open-source software, which makes them ideal for the trials described in this paper. The software on the pixhawks in the multirotors have been slightly modified with regards to controller inputs. The modifications are available online.[1]

The onboard computer is a Beaglebone Black (Beagleboard, 2013) running the LSTS software toolchain (Pinto et al., 2013). The Beaglebone is a versatile embedded linux development board, offering plenty of

[1] https://github.com/krisklau/ardupilot/tree/copterdev/3.3

IO[2], accompanied by a 1 GHz ARM Cortex-A8 CPU. The LSTS toolchain is the core software suite used for implementation and realization of the described recovery maneuver. The toolchain consists of a minimal Linux distribution (Glued), a software framework layer (DUNE), and a ground control segment (Neptus). It is all open-source, and available online (Github.com, 2016). The toolchain is highly expandable, and makes it relatively easy to add new controllers to the underlying framework. It is designed to handle distributed heterogeneous vehicles operating in the same environment, which when accompanied with a dedicated GCS makes it a better alternative for complex operations than other available frameworks.[3] All the controllers discussed in this paper are implemented in C++ in DUNE.

The communication to the Pixhawk from the Beaglebone is done using the *MAVLink* protocol (MAVlink.org, 2017) over a serial interface (UART) running at 912000 kb/s baud rate. Attitude and other telemetry data is transmitted from the pixhawk at 25 Hz, with a measured maximum latency of 30 ms. As depicted in Figure 9, DUNE transmits desired acceleration (labeled as $\mathbf{F}_i$, see also (2)) in the inertial coordinate frame to the pixhawk, which calculates the resulting desired roll- and pitch-angle and total thrust.

As discussed, the accuracy of RTK GPS is required for the recovery maneuver. We leverage the open-source library RTKlib (Takasu and Yasuda, 2009), which enables us to build a low-cost cm-level accurate positioning system. Accompanied by the uBlox M8T raw GNSS receiver and a slightly modified version of RTKlib[4], we are able to measure position and velocity of all the UAVs at 10 Hz. RTKlib runs alongside DUNE on Beaglebone, and the RTKlib configurations are also available online.[5]

The choice of antennas are critical for successful operations with RTK GPS. Even though patch-antennas with a suitable ground plane are most common for UAVs, we have opted for a helical active L1 antenna from Maxtena which has a very low weight and does not require a ground plane. In our tests they have shown superior performance on the tilting UAV platforms.

Although our controllers receive precise position data from the RTK GPS at 10Hz, due to the calculation times of RTKlib and propagation delay from the GPS receiver the data is available with a total delay of approx. 200 ms. This puts a restriction on the maximum achievable bandwidth of the controllers. By fusing the data with inertial- or other sensors, this delay can be compensated for, but this is not done in this work. However, the achievable bandwidth proved sufficient for the proposed control architecture and the experiments conducted for this article.

Communication between all vehicles (fixed-wing UAV, multirotors) and the ground control station is through a wireless network solution developed by Ubiquity Networks[6]. Specifically, the *Ubiquity Rocket M5* provides a 5.8 GHz wireless network with the AIRMAX transmission protocol. This is a *Time Division Multiple Access* (TDMA) network, providing constant throughput with minimal latency variance, which is important for the coordinated control strategies proposed in this article. The radio is interfaced through a standard RJ45 ether net plug, providing a bridged interface to the network.

[2]Inputs and Outputs, such as serial lines (UART), SPI and General Purpose Input Output (GPIO).
[3]For instance the also excellent *Robot Operating System*(ROS), which has a broad user base in the scientific community.
[4]https://github.com/krisklau/RTKLIB/tree/fix/iss99
[5]https://github.com/LSTS/glued/blob/master/systems/ntnu-b2xx/fs/etc/rtklib/conf/rtkrcv.conf
[6]http://ubnt.com

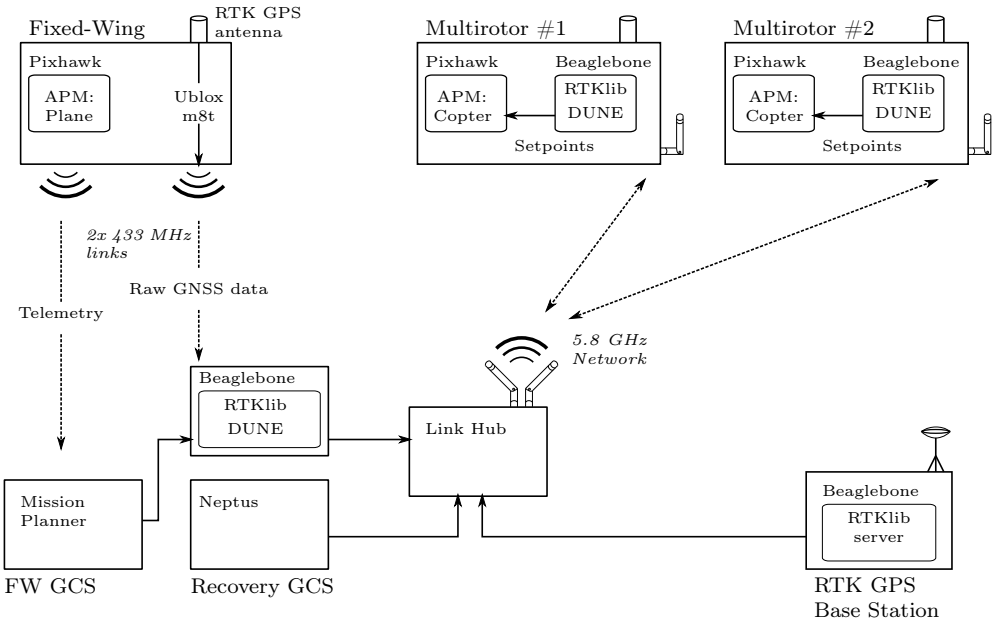

Figure 10: Detailed communication diagram for the experimental setup. In addition to the on-board autopilots, the setup consists of four Beaglebone Black's for onboard and ground processing, ground control stations and a wireless network from Ubiquity Networks.

4.3 Net, Support Structures and Sensors

The net under the multirotors is attached to a flexible aluminum rod both at the bottom and top of the assembly, as seen in Figure 1. The rod helps to stretch out the net, and also works as a shock-absorber during the impact with the fixed-wing UAV. Lastly, it will make sure that most of the forces from lifting the fixed-wing UAV after recovery is directed downwards, rather than inwards, which would cause the multirotors to spend unnecessary energy to stay apart from each other.

To choose the net for the setup, various alternatives were explored. It is important to keep the weight low, and it additionally needs to be strong enough to last for several recovery maneuvers. In the end, we chose a very light-weight ($<$40 g) net made from nylon threads, each at the thickness of a regular fishing-line, originally intended to keep birds away from berry-bushes. The net is 5 by 3 m.

After the fixed-wing UAV has made contact with the net, some mechanism is needed for it to stay attached. As can be seen in Figure 11, we rigidly attached two metallic rods to the nose of the UAV, and bent them once to act as a simple hook. This proved to be very effective, with little intrusion on the fuselage and flight performance. Similar hooks could also be applied to the wings of the UAV, to enable even more robust linkage to the net.

To attach the net to the multirotors, a multi-purpose attachment device was created, see Figure 11. It consists of (1) a quick-release mechanism, and (2) a tension sensor. The quick-release mechanism is built around a cylinder with a circular release pin. This design, combined with a smooth nylon-coated wire attached to the top of the net, allows for a low-friction operation which can be driven by a micro-sized (4.7 g) servomotor, even with several kg's of load. The tension-sensor is a low-weight load-cell from Futek, LSB200 (Futek.com, 2016). The combined assembly is installed on a gimbal-like structure to facilitate free range of motion, so that the load cell is only subjected to external forces along it's sensor line as illustrated in Figure 11.

Figure 11: Left: Metallic hooks attached to the nose of the fixed-wing UAV, used to latch onto the suspended net. The hooks had little to no effect on flight performance. Right: Assembled quick-release mechanism and tension sensor on a gimbal-like structure for free range of motion.

4.4 Ground Control Station

To control the recovery maneuver, the operator is presented with an overview of the location of the recovery maneuver, as seen in Figure 12. Here the operator can set the height and width of the virtual runway (works as a fence for the location of the multirotors) prior to the maneuver, as well as monitor the progress with the location of all vehicles while the recovery is taking place. In addition to the sky-view, the operator can also see the location of the vehicles in the cross-track plane, which is very useful for the initial tuning of the maneuver parameters. These views are extensions to the GCS in the LSTS toolchain as discussed in Section 4.2

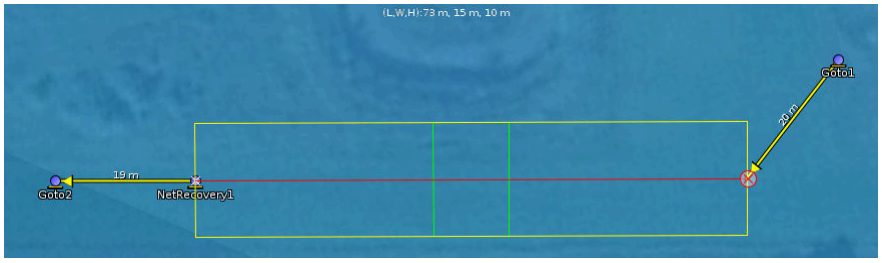

Figure 12: Zoomed-in view of the operator interface for the net-recovery maneuver. The yellow rectangle represents the safety area (width of the virtual runway), while the green lines represent the location of the planned recovery.

4.5 Controller Tuning

To tune the controllers, several fixed-wing recovery maneuvers were conducted without the actual net between the multirotors, and an additional 5 m of offset distance was put in place. This allowed safe operations while tuning and assessing the performance of the system. The whole system has three tuning profiles: *Cruise*, *Normal*, and *High Gain*, which are in use during transport, approach and final recovery phase, respectively. Additionally, as described in Section 3.3.1, a faster 2nd order trajectory generator is in use in the *High Gain* phase.

Overall, the formation controller was to a higher bandwidth than the cross-track coordination controller, and a high relative damping factor was used to ensure smooth operations and to better react to the abrupt force from the incoming fixed-wing UAV.

4.6 Operational Aspects

As this is a rather complex experiment, involving three flying vehicles, it is vital to have a well-grounded operational environment. Three UAV pilots were involved in the operation, each responsible for a separate vehicle and able to take control. The operation was conducted as follows:

Pilot A conducted a manual takeoff of the fixed-wing UAV using an RC transmitter. After reaching cruising altitude, a rectangular flight-plan (see Figure 13) which included the recovery location was uploaded and initiated on the fixed-wing autopilot. On-board battery fail-safe systems monitor the fixed-wing UAV battery capacity. The two multirotor UAVs was positioned on the ground, with the net between them. A pilot-assisted control mode is then initiated, which allows a single pilot, Pilot B, to take-off and maneuver the two multirotor UAVs in a synchronous fashion. In reference to Figure 6, the pilot sets the desired *mission velocity* using an RC-remote controller. After takeoff, Pilot B issues a command for the autonomous recovery maneuver to start, in which the multirotor UAVs move towards the start of the virtual runway, awaiting the approaching fixed-wing UAV. At all times, Pilot B and Pilot C are able to take manual control of multirotors 1 and 2, respectively. The procedures for this, along with a number of other safety systems, are discusses in the next section.

After the autonomous recovery is completed, the multirotors return with the fixed-wing UAV to the start of the virtual runway. There, they await for the pilot to give command to enter the pilot-assisted control mode again. Then, the single pilot guides the multirotor toward the landing area. When the now suspended fixed-wing UAV is lowered to the ground, the pilot releases the net with a switch on his RC transmitter. Pilot B and Pilot C then lands the multiorotors individually.

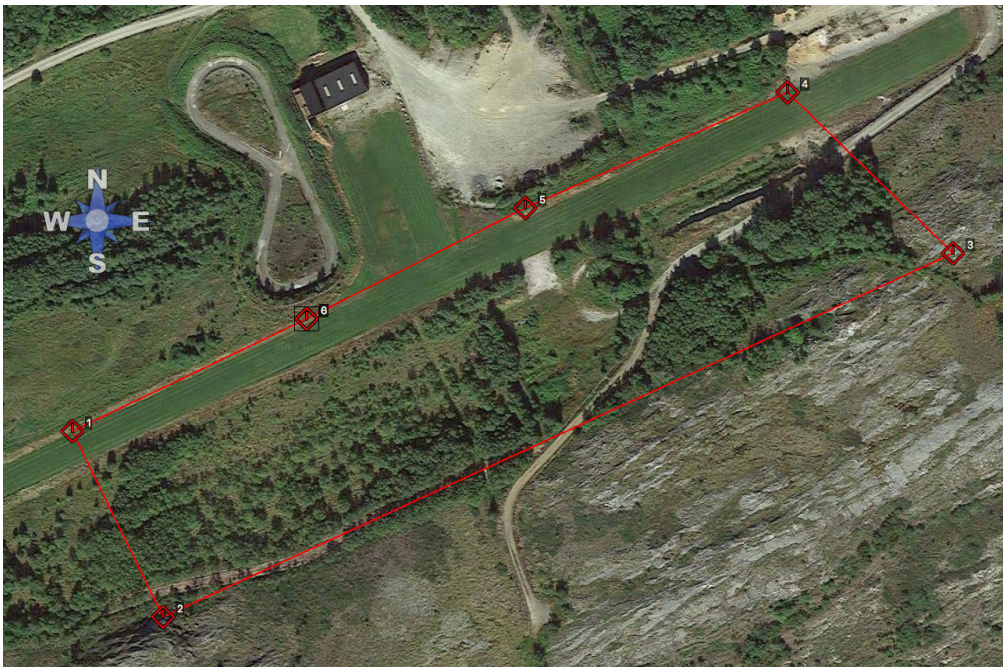

Figure 13: Nominal flight-plan for the fixed-wing UAV during the experiments. The designated recovery location is in the middle of the grass runway, on the upper long leg of the path.

4.6.1 Safety

In accordance with the local civil aviation authorities, these tests was categorized as conducted within *Visual Line Of Sight* (VLOS), and were coordinated with the nearby air traffic control tower. At all times, a pilot

has the capability to resort to manual control, using an RC transmitter to the autopilot, of each aircraft should it be needed.

A number of automatic failsafe systems were put in place. To simplify the operational aspects during these trials, any of the following conditions triggered an *abort*. Should such an abort be triggered, the two multirotors would (1) simultaneously drop the suspended net, and (2) move 3 m directly away from each other, using control-logic on the low-level autopilot. There, the multirotors would wait until manual control is issued by the pilot. The following conditions triggers an *abort*:

- *Pilot abort*: Each pilot has a RC transmitter with a dedicated button to manually trigger an abort, should the need arise due to unforeseen events.

- *Battery capacity*: Battery voltage and remaining capacity is monitored by the autopilot. If the level reaches a certain lower bound, a battery-failsafe is triggered.

- *Weight of suspended load*: During recovery, should the weight on a single multirotor from the suspended load be measured to be over 1.5 kg for more than 0.5 s, a weight-failsafe is triggered.

- *Communication timeout*: Should the communication link between any of the vehicles or ground control station drop out for more than 0.5 s, the position and velocity information between the vehicles can no longer be updated, and a timeout-failsafe is triggered.

- *RTK GPS lock loss*: The system relies on the accurate positioning solution of the RTK GPS for precision recovery of the incoming fixed-wing UAV, and maintaining relative formation between the multirotors. Should the navigation solution lose lock, either due to communication failure with the base station, satellite obstruction, numerical calculation errors or other events, an abort is triggered. Note that the system permits a short (1 s) loss of lock, in which a navigation algorithm augments the location solution from a standard secondary code-based GPS with the last valid RTK GPS solution before issuing the abort.

The ground control station would inform the operator of the source of the abort signal. Although the failsafe-procedures uses straight-forward condition-based logic that all led to the same abort event, it provided a robust platform for experimental tests. Naturally, more logic could be added in the future. As an example, two levels of battery failsafes levels could be added, where only the lower critical one would trigger a drop of the suspended load, useful to prevent unwanted release of the fixed-wing UAV just after the recovery, but before being lowered to the ground.

In the experimental trials conducted, the length of the timeouts discussed above was chosen rather conservatively. In a operational scenario, longer periods of communication dropout and loss of RTK GPS lock can be tolerable, depending on the specific situation. For instance, in the case of communication loss between the fixed-wing UAV and the multirotor UAVs, a wait-and-hold pattern can be initiated until communication is re-established. Secondary short-range links can be used for redundancy and transmission of critical data between the multirotors to ensure reliability, and deeper integration with inertial sensors can lead to better precision during loss of RTK GPS lock using a standard code-based GPS as a fallback solution.

Further, the three pilots used was needed to ensure safe trials during the test-phase. As the system is designed to be fully autonomous, the number of pilots can readily be reduced. A single pilot can be used, assisted by the on-board controller software, to guide the multirotor UAVs during takeoff and landing. As the fixed-wing UAV is on respectively on autopilot or recovered in the net, the same operator crew used in the fixed-wing operation can be used for the recovery maneuver.

5 Results

Experiments were conducted to test the proposed maneuver in December of 2016 in Trondheim, Norway. The temperature was a brisk 2 °C, with a fairly calm wind of approx. 3-4 m/s, and some stronger gusts. In preparations for the actual recovery maneuver, several trial runs were conducted using all assembled equipment except for the net. That way, we could test the setup and tuning of the controllers prior to performing the recovery maneuver as described in Section 4.6. Snapshots of one of the experiments can be seen in Figure 14.

The fixed-wing UAV was set to continuously fly a rectangular pattern with an altitude of 40 m to stay clear of the surrounding trees and hills. One of the long legs corresponded to the desired landing area, in which the UAV descended to an altitude of approx. 10 m. The cruise-speed of the UAV was 16 m/s, while at the landing zone it had a designated speed of 12 m/s. The resulting flight-path of the fixed-wing UAV has some natural variation due to the use of single-precision code-based GPS for navigation, which can be observed in Figure 15.

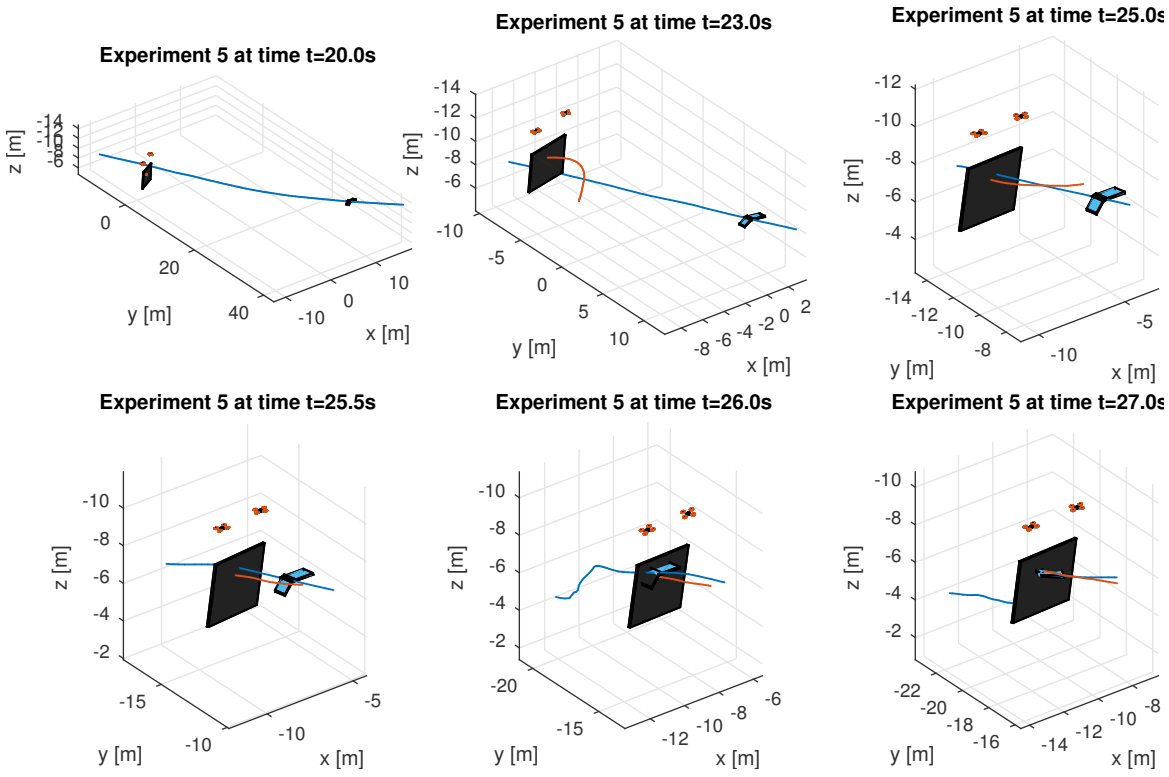

Figure 14: Snapshots of the recovery maneuver from Experiment 5, which shows the movements of the vehicles before and during the recovery. The illustrations are renderings from the data logged during the experiment. The blue line represents the trajectory of the fixed-wing UAV as recorded by the on-board RTK GPS, while the red line is the trajectory of the calculated net-position up until the snapshot time.

A total of five attempts at autonomous recovery of the fixed-wing UAV using two coordinating multirotors were conducted. Of the five tests conducted, four resulted in a successful recovery of the fixed-wing UAV. For the remaining experiment, excessive lateral movements and a structural weak point in the net caused only the wing to make contact, thus resulting in the fixed-wing UAV not attaching to the net. However, it continued its nominal flightpath unharmed. The lateral movements of the fixed-wing UAV took place the moment before recovery, most likely caused by a strong wind gust. This can be seen at the very end of Figure 17. By applying hooks to the wings as well, this attempt would also have been successful. Also, a more aggressively tuned or larger fixed-wing UAV would be less affected by the such wind gusts, should they appear just before the recovery. The multirotor UAVs were successful in tracking the variations in the

fixed-wing flight path leading up the unsuccessful recovery, as well as on the other successful ones.

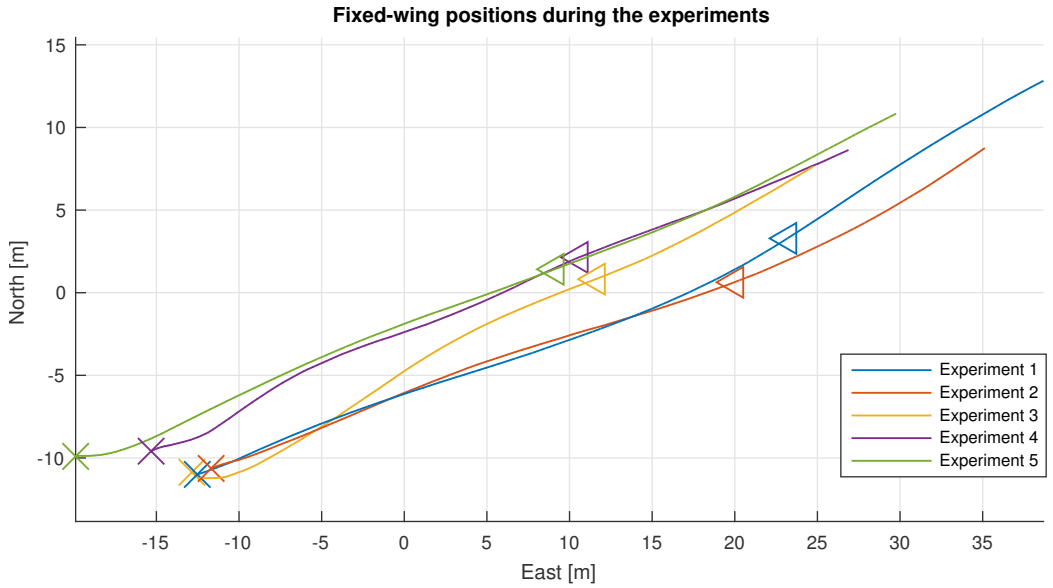

Figure 15: Flight-path of the fixed-wing UAV just prior to the recovery in the net. The figure illustrates the accuracy and behavior of the path-controller in the low-level fixed-wing UAV autopilot. Note that the fixed-wing UAV does not alter its path based on the location of the net; it is up to the multirotors to use position and velocity data to intercept and recover the incoming fixed-wing UAV. The cross and triangle marks the time of recovery and start of multirotor *high gain* phase, respectively.

A video illustrating the successful recovery of the fixed-wing UAV is available online.[7]

Figure 14 shows an overview of one of the experiments conducted. We can see the two multirotors waiting with the suspended net for the fixed-wing UAV to approach. When it is close, the multirotors starts the crosstrack tracking as to intercept the path of the incoming fixed-wing UAV. We see that in both cases the multirotors are able to intercept and successfully recover it.

To show the performance of the control algorithms, the results from all five experiments are assembled in Figure 16. Here, the *relative position* of the net and fixed-wing UAV is shown at the top, while the bottom part shows the distance from the fixed-wing UAV to the *net edge* in the cross-track plane.

Figure 17 shows how the net position is tracking the position of the fixed-wing UAV in the y-component of the crosstrack plane in the virtual runway. The marked triangle represents the point were we enter a *high gain* profile, where 3rd order trajectory generator is replaced with a faster 2nd order one.

In Figure 18, the cable tensions for two of the experiments are shown. The tension was measured using on-board strain gauges, as described in Section 4.3. It can be seen that at the moment the fixed-wing UAV makes contact with the suspended net, a peak tension of approximately 2.5 kg is measured. However, it relatively quickly settles to the resting mass of the now suspended fixed-wing UAV. At the end of the time-series, it is seen how the weight drops to zero when the plane is put to rest on the ground, and the net is released.

6 Conclusion and Final Remarks

In this article, we have presented a novel method for autonomous recovery of fixed-wing UAVs using a net suspended below two multirotor UAVs. The proposed method enables fixed-wing UAV operations in the

[7] `https://youtu.be/IZJt3WvFZbE`

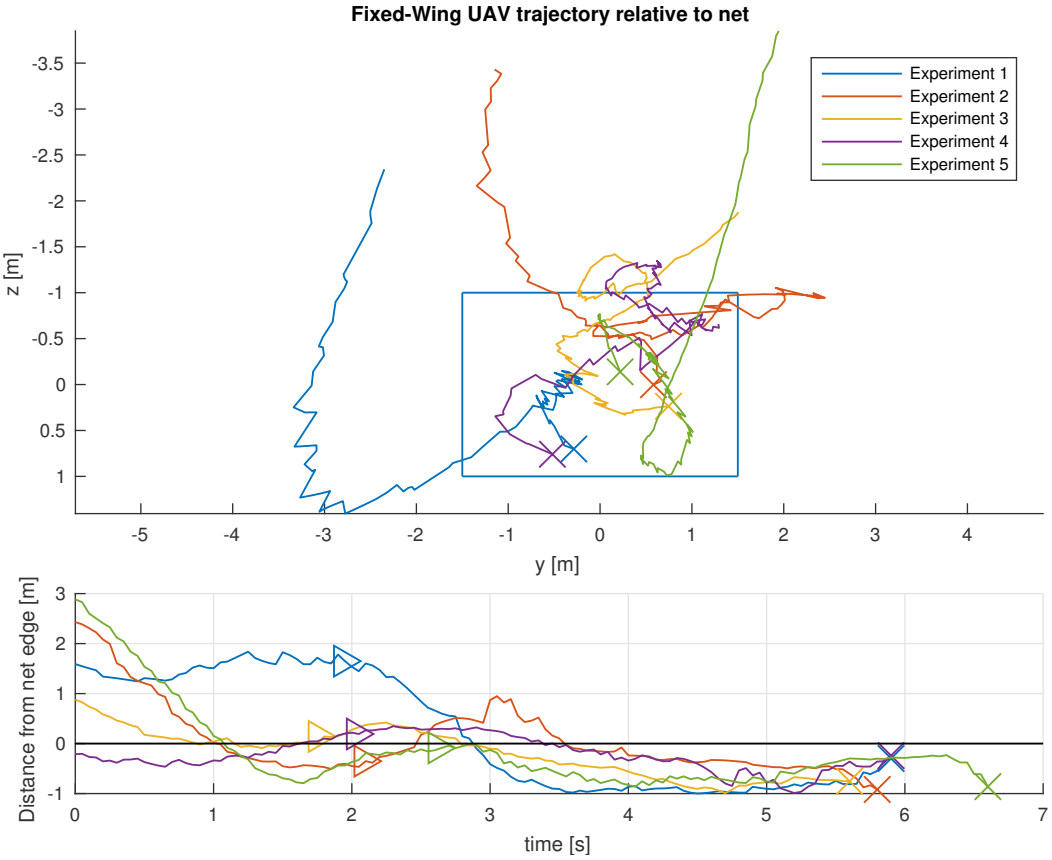

Figure 16: Tracking results from all five recovery attempts. Even though experiment three was unsuccessful in firmly attaching the fixed-wing UAV to the net, the data still shows adequate tracking performance. Note that the upper part illustrates the *relative* position of the fixed-wing UAV and the net (blue square) in the crosstrack plane.

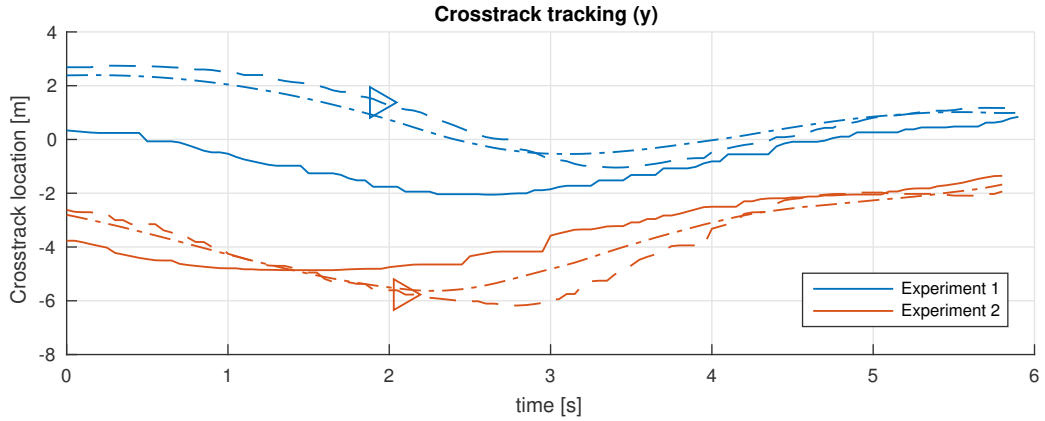

(a) Crosstrack tracking performance in the y-direction for the first two experiments.

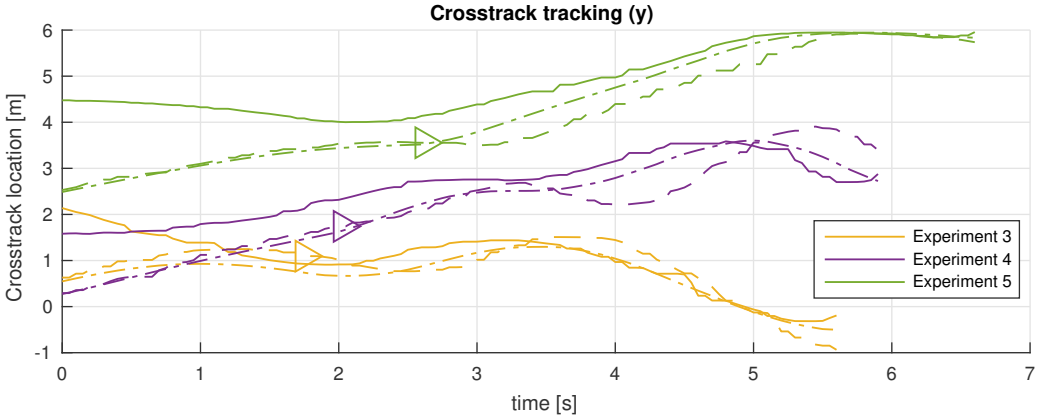

(b) Crosstrack tracking performance in the y-direction for the last three experiments.

Figure 17: Crosstrack tracking performance for (a) the first two experiments, and (b) the last three experiments. Relative to experiments 1& 2, the damping parameter in the tracking generator was adjusted slightly in the last three, resulting in better performance. The solid line is the fixed-wing UAV position, while the dashed and dash-dotted line represents the net location and trajectory generator output, respectively. The triangle position mark the moment in time when the *high gain* control profile is activated.

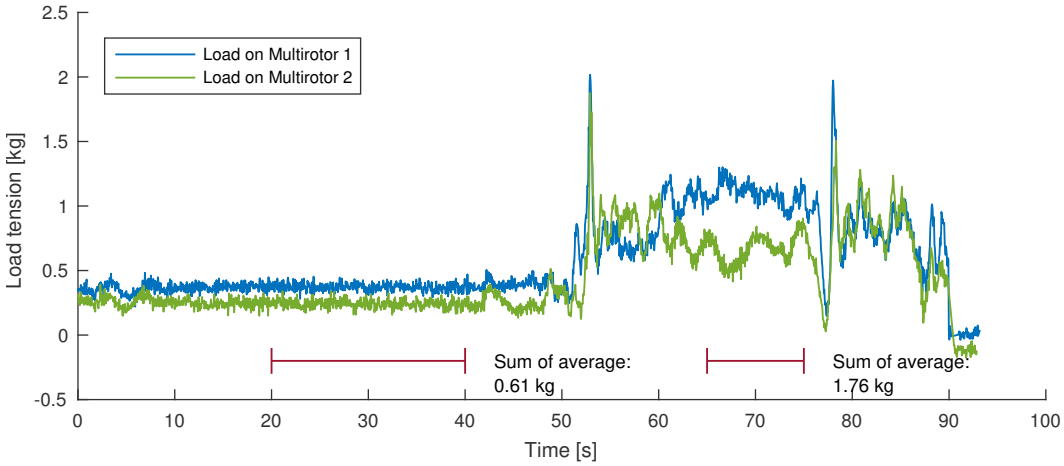

(a) Cable tension during Experiment 1

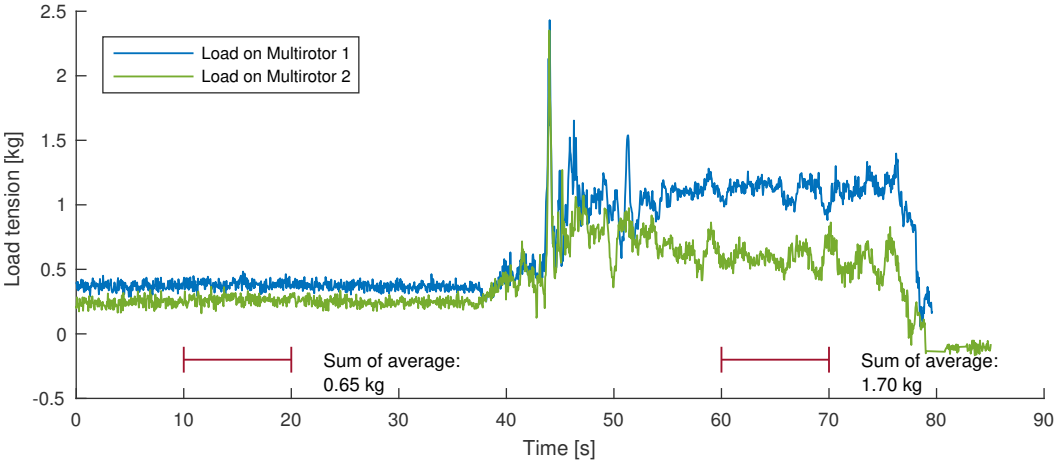

(b) Cable tension during Experiment 4

Figure 18: Cable tension on both multirotors for experiments 1 (a) and 4 (b). In both cases, the initial wait time shows a constant weight of roughly 0.6 kg, which represents the total weight of the net + structure rod assembly. A peak force of about 2.5 kg on each multirotor is measured just as the fixed-wing UAV enters the net. After a brief settling time, the total weight settles to approximately 1.7 kg, which matches well to the weight of the fixed-wing UAV. The average weight-calculations is done on the data as marked in the figure. The second peak in (a) is due to a operator error during takeover to semi-manual control prior to landing, which caused a brief, rapid downwards deceleration.

absence of runways or sufficient space for a stationary net. It is especially suited for ship-based marine launch and recovery operations, as the wave-induced heave motion of the ship, and other environmental factors does not affect the recovery, as it is conducted off the ship deck. In addition, the recovery maneuver can be readily adapted to changing wind conditions and direction.

A complete control system was proposed, along with the definition of a *virtual runway* for which the recovery maneuver is performed along. The proposed control system includes cooperative formation control algorithms of the two multirotors, and a trajectory generator to track and intercept the incoming fixed-wing UAV.

Multiple experimental trials were conducted on a smaller-scale fixed-wing UAV to validate the proposed control system. The recovery maneuver was conducted fully autonomously, for which the control algorithms were implemented on-board each UAV in a distributed fashion. The experimental platform included the use of Real-time kinematic GPS for precise navigation solutions.

Although the experimental platform used consisted of a small scale fixed-wing UAV (~ 1.2 kg), the proposed control system is directly applicable to larger systems.

Acknowledgments

This work was partially supported by the Research Council of Norway through its Centers of Excellence funding scheme, grant number 223254 (NTNU Centre for Autonomous Marine Operations and Systems).

The authors would like to thank the UAV operators Lars Semb and Pål Kvaløy, for their invaluable aid in preparing and performing the experiments. The first author would also like to thank Jostein Borgen Moe, Joathan Cornel van den Hoorn and Alojz Gomola, for their aid in the initial part of the implementation during their MSc. thesis work and internships.

References

Arcak, M. (2007). Passivity as a Design Tool for Group Coordination. *IEEE Transactions on Automatic Control*, 52(8):1380–1390.

Arcak, M., Teel, A., and Kokotovic, P. (2001). Robust nonlinear control of feedforward systems with unmodeled dynamics. *Automatica*, 37:265–272.

Ardupilot.com (2016). Ardupilot - Open source autopilot.

Bai, H., Arcak, M., and Wen, J. T. (2011). *Cooperative control design: A systematic, passivity-based approach.* Springer-Verlag New York.

Beagleboard (2013). Homepage of the BeagleBone project: http://beagleboard.org.

Beard, R. W. and McLain, T. W. (2012). *Small Unmanned Aircraft: Theory and Practice.* Princeton University Press.

Delftdynamics.nl (2015). DroneCatcher catches drone.

Futek.com (2016). LSB200 S-Beam.

Github.com (2016). LSTS: Underwater Systems and Technology Laboratory.

Kim, H. J., Kim, M., Lim, H., Park, C., Yoon, S., Lee, D., Choi, H., Oh, G., Park, J., and Kim, Y. (2013). Fully autonomous vision-based net-recovery landing system for a fixed-wing UAV. *IEEE/ASME Transactions on Mechatronics*, 18(4):1320–1333.

Klausen, K., Fossen, T. I., and Johansen, T. A. (2014). Suspended Load Motion Control using Multicopters. In *Proceedings of the Mediterranean Conference of Control and Automation (MED)*, pages 1371–1376, Palermo. IEEE.

Klausen, K., Fossen, T. I., and Johansen, T. A. (2017). Nonlinear Control with Swing Damping of a Multirotor UAV with Suspended Load. *Journal of Intelligent & Robotic Systems*.

Klausen, K., Moe, J. B., Van Den Hoorn, J. C., Gomola, A., Fossen, T. I., and Johansen, T. A. (2016). Coordinated Control Concept for Recovery of a Fixed-Wing UAV on a Ship using a Net Carried by Multirotor UAVs. In *Proceedings of the 2016 International Conference on Unmanned Aircraft Systems (ICUAS)*, pages 964–973.

Laiacker, M., Kondak, K., Schwarzbach, M., and Muskardin, T. (2013). Vision aided automatic landing system for fixed wing UAV. *Proceedings of the IEEE International Conference on Intelligent Robots and Systems*, pages 2971–2976.

Mahony, R., Kumar, V., and Corke, P. (2012). Modeling, Estimation, and Control of Quadrotor. *IEEE Robotics and Automation Magazine*, 19(3):20–32.

MAVlink.org (2017). MAVLink Micro Air Vehicle Communication Protocol.

Meissen, C., Klausen, K., Arcak, M., Fossen, T. I., and Packard, A. (2017). Passivity-based Formation Control for UAVs with a Suspended Load. In *Proceedings of the IFAC World Congress*.

Mtu.edu (2016). Michigan Tech Robotic Falconry.

Muskardin, T., Balmer, G., Persson, L., Wlach, S., Laiacker, M., Ollero, A., and Kondak, K. (2017). A Novel Landing System to Increase Payload Capacity and Operational Availability of High Altitude Long Endurance UAVs. *Journal of Intelligent and Robotic Systems: Theory and Applications*.

Nextgenerationvision.fr (2014). Drone interception.

Pinto, J., Dias, P. S., Martins, R., Fortuna, J., Marques, E., and Sousa, J. (2013). The LSTS toolchain for networked vehicle systems. In *Proceedings of the MTS/IEEE OCEANS*, Bergen. MTS/IEEE.

Pixhawk.ethz.ch (2016). PX4 Pixhawk.

Richardson, T. S., Jones, C. G., Likhoded, A., Sparks, E., Jordan, A., Cowling, I., and Willcox, S. (2013). Automated vision-based recovery of a rotary wing unmanned aerial vehicle onto a moving platform. *Journal of Field Robotics*, 30(5):667–684.

Rife, J., Khanafseh, S., Pullen, S., De Lorenzo, D., Kim, U. S., Koenig, M., Chiou, T. Y., Kempny, B., and Pervan, B. (2008). Navigation, Interference Suppression, and Fault Monitoring in the Sea-Based Joint Precision Approach and Landing System. *Proceedings of the IEEE*, 96(12):1958–1975.

Serra, P., Cunha, R., Hamel, T., Cabecinhas, D., and Silvestre, C. (2016). Landing of a Quadrotor on a Moving Target Using Dynamic Image-Based Visual Servo Control. *IEEE Transactions on Robotics*, 32(6):1524–1535.

Skulstad, R., Syversen, C., Merz, M., Sokolova, N., Fossen, T., and Johansen, T. (2015). Autonomous Net Recovery of Fixed-Wing UAV with Single-Frequency Carrier-Phase Differential GNSS. *Aerospace and Electronic Systems Magazine, IEEE*, 30(5):18 – 27.

Takasu, T. and Yasuda, A. (2009). Development of the low-cost RTK-GPS receiver with an open source program package RTKLIB. In *Proceedings of the International Symposium on GPS/GNSS*, Jeju, Korea.

Teel, A. R. (1992). Global stabilization and restricted tracking for multiple integrators with bounded controls. *Systems & Control Letters*, 18(3):165–171.

Theverge.com (2015). Tokyo police unveil net-wielding interceptor drone.

Thurrowgood, S., Moore, R. J. D., Soccol, D., Knight, M., and Srinivasan, M. V. (2014). A biologically inspired, vision-based guidance system for automatic landing of a fixed-wing aircraft. *Journal of Field Robotics*, 31(4):699–727.

Venugopalan, T. K., Taher, T., and Barbastathis, G. (2012). Autonomous landing of an Unmanned Aerial Vehicle on an autonomous marine vehicle. *Proceedings of the 2012 MTS/IEEE OCEANS*.